Kagawa and Noguchi
Earth, Planets and Space (2022) 74:74
https://doi.org/10.1186/s40623-022-01640-3

Earth, Planets and Space

EXPRESS LETTER

Open Access

Issues related to velocity structure estimation in small coastal sedimentary plains: case of Tottori plain facing the Sea of Japan

Takao Kagawa* and Tatsuya Noguchi

Abstract

Issues of predominant period of ground motion and derived underground velocity structure model are investigated in the coastal plains affected by the shallow soft sedimentary layer after the last ice age. It is found that two predominant periods due to the shallow soft layer and deeper drastic sedimentary boundaries are close in a small plain such as the Tottori plain, Japan as an example. This study analyzes the underground velocity structure derived from EHVSR (*H/V* spectrum ratio of earthquake ground motions) with the diffuse field theory. It is considered that the interaction of close predominant periods due to the different layer boundaries with high contrast may amplify the seismic ground motion in the period range that affects building structures in small plains in coastal area.

Keywords: Small coastal plain, Predominant period, Velocity structure, Diffuse field theory, Tottori plain

Graphical Abstract

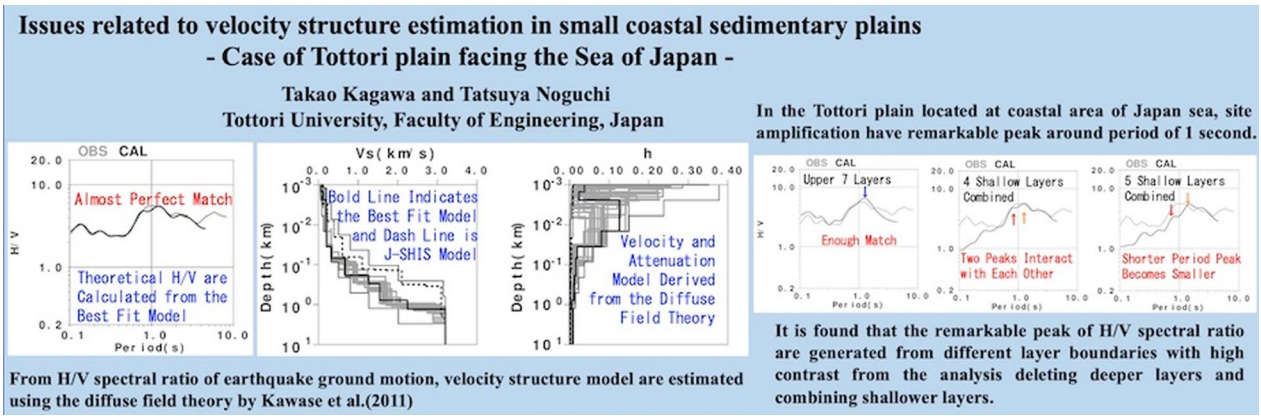

Introduction

In the coastal plains, the soft layer deposited by Holocene transgression, beginning from the end of the last ice age, has generated a notable predominant period, which is generally shorter than 1 s at the boundary with engineering bedrock (predominant period T1). The plains

*Correspondence: kagawa@tottori-u.ac.jp

Faculty of Engineering, Tottori University, 4-101 Koyamacho-Minami, Tottori, Japan

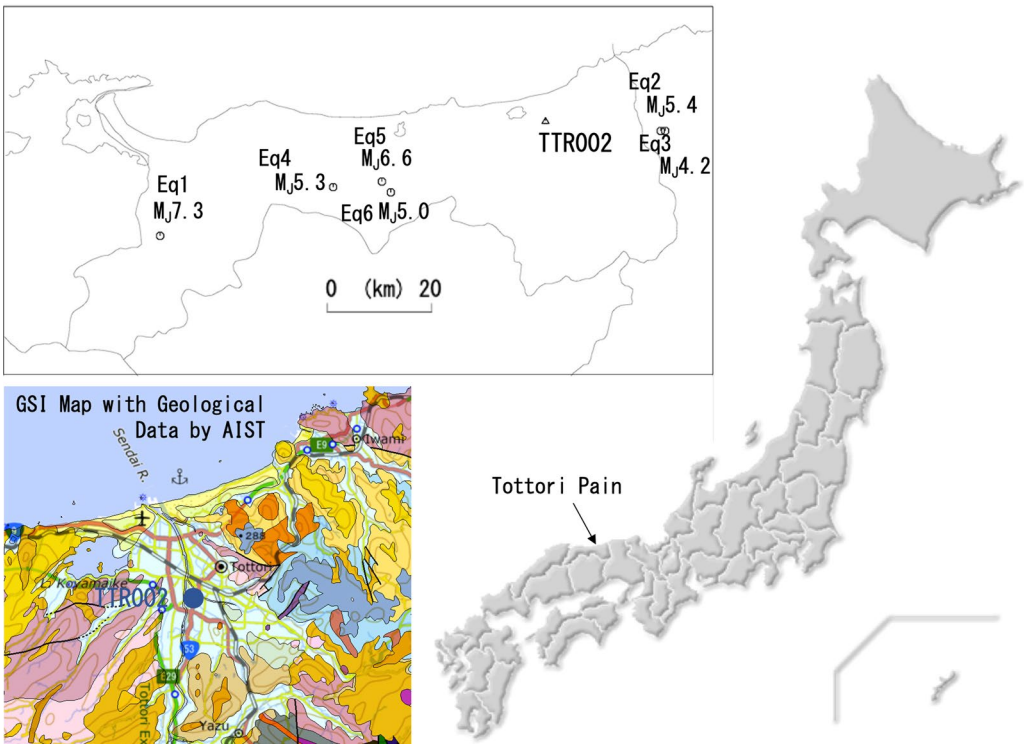

Fig. 1 Location of Tottori plain and target site TTR002 with epicenter distribution of earthquakes used in the study. Earthquake numbers are common with those in Fig. 2a. Geological map in left bottom panel shows the area of Tottori plain (lime green)

and basins in Japan have been affected by tectonic movements during the Quaternary period and have deposited thick sedimentary layers in the area, and are relatively subsided from the surrounding mountains. Another notable predominant period is formed by the high contrast at deep sedimentary boundaries with the seismic bedrock (predominant period T2).

It is well known that large sedimentary basins such as the Kanto, Nobi, and Osaka plains have thick sedimentary layers over the seismic bedrock, and their T2s are of several seconds. The predominant period of Osaka basin is around 6 s (e.g. Kagawa et al. 2004; Tsai et al. 2017), while that of Kanto Plain is around 8 s (e.g. Yamanaka and Yamada 2006; Yoshimoto and Takemura 2014). These predominant periods are much longer than T1s that are expected in the respective areas. However, in small plains such as the Tottori plain, Japan (Fig. 1), the sediment on the seismic bedrock is thinner in comparison to the large plains, and T2 might not be long enough to be differentiated from T1. It is expected that the amplified interference of T1 and T2 may cause generation of a large peak in site response. There are studies that have investigated site responses of small basins, but their focus has been on the influence of surface waves due to irregular boundary structure (Uetake and Kudo 2005; Kanno and Miura 2006) or non-linear soil response (Bonilla et al. 2006). Studies related to the effect of different predominant periods occurring due to the different layer boundaries have been uncommon.

Therefore, in this work we have tried to emphasize on the effects that were observed in EHVSR (H/V spectrum ratio of earthquake ground motions) in the Tottori plain. Diffuse field theory (Kawase et al. 2011) is applied to EHVSR at a strong ground motion observation site in the Tottori plain to estimate the velocity structure model, and after verification of its validity, the contribution of layer boundaries to the predominant periods is studied.

Estimation of velocity structure from *H/V* of earthquake ground motion

The TTR002 site of K-NET (National Research Institute for Earth Science and Disaster Resilience 2019a) is selected as the target site in the Tottori plain. Six records were made with an epicentral distance of 100 km or less and a PGA of 10–100 cm/s^2. These records are not affected by non-linear ground responses as their PGAs are smaller than 100 cm/s^2 (e. g. Idriss 1991). The records are of, the 2000 western Tottori prefecture earthquake (M_J 7.3), the 2016 Central Tottori prefecture earthquake (M_J 6.6), and other four earthquakes having M_J between

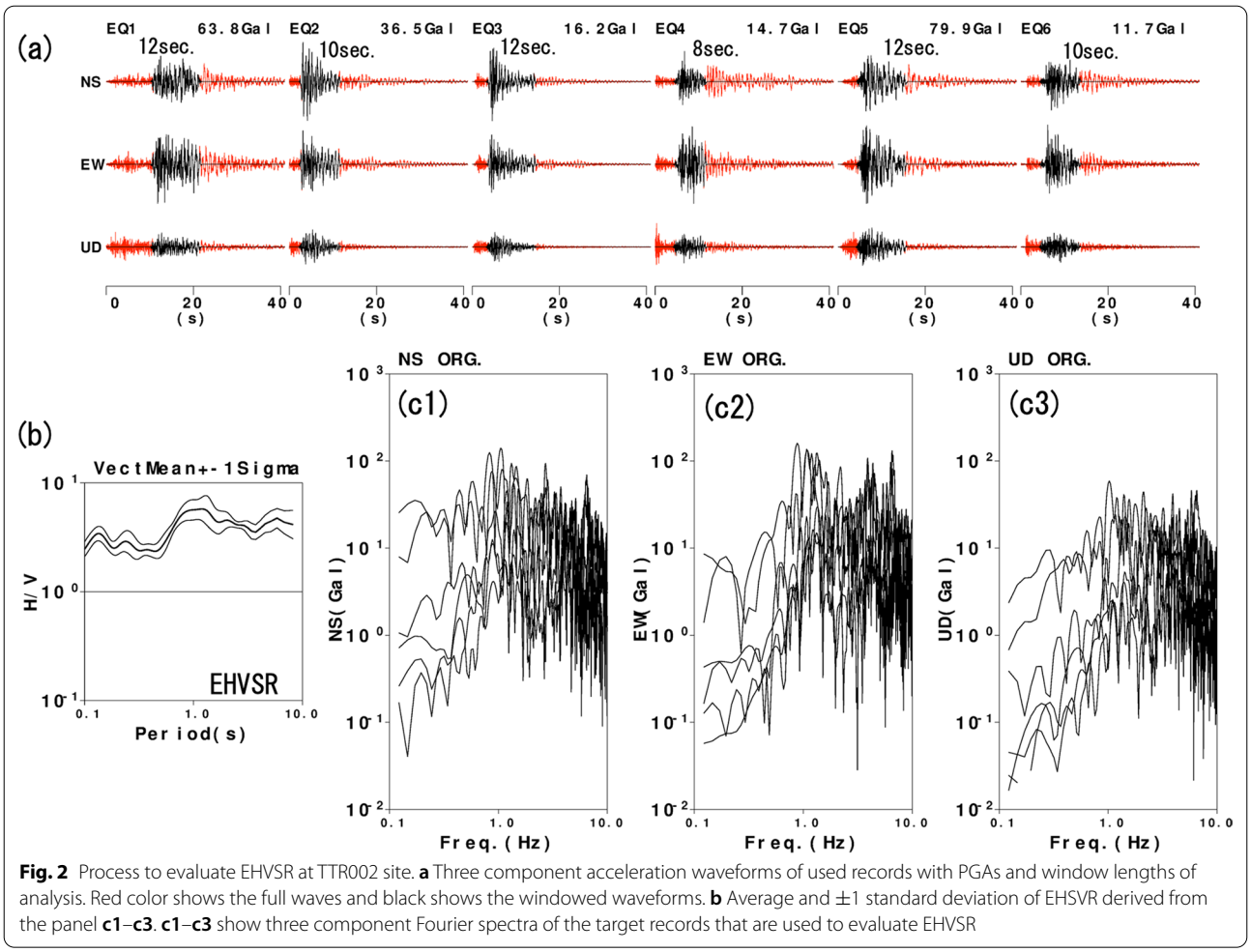

Fig. 2 Process to evaluate EHVSR at TTR002 site. **a** Three component acceleration waveforms of used records with PGAs and window lengths of analysis. Red color shows the full waves and black shows the windowed waveforms. **b** Average and ±1 standard deviation of EHSVR derived from the panel **c1**–**c3**. **c1**–**c3** show three component Fourier spectra of the target records that are used to evaluate EHVSR

4.2 and 5.4. The locations of the epicenters are shown in Fig. 1. The averaged EHVSR is obtained from three component observation records for 40.96 s. However, time windows of 8–12 s have been applied to mainly use the S wave portion, and to neglect the effects of surface waves. Figure 2a shows the waveforms with PGA and window lengths. Figure 2b shows the average with plus and minus one standard deviation of EHVSR derived from Fourier spectra in Fig. 2c1–c3. Vector sum of NS and EW components is used to evaluate the horizontal component and the EHVSR is smoothed using the filter proposed by Konno and Ohmachi (1995) which provides same smoothing effects over the entire frequency range in logarithmic axis. The EHVSR has a remarkable peak around 1 s, and the standard deviation is small for a wide range of the period. A small increment is found in the longer period range of over 5 s. This increment, however, might be affected by Lg waves (Furumura et al. 2003) that are not completely removed by the time windows, as observable in Fig. 2a. Then, the following analysis targets up to 5 s. The gray line in Fig. 3a shows the average EHVSR in Fig. 2b. As a reference, MHVSR (H/V spectrum ratio of microtremor measurement) evaluated close to the observation point is shown in Fig. 3b. Both, EHVSR and MHVSR, follow similar trends, but their peaks differ, where EHVSR has a higher peak value than MHVSR. In addition, the peak of MHVSR appears around 0.6–0.8 s, which seems to be slightly shorter than that of EHVSR. The reason behind this could be that the power of a microtremor is not large enough to give rise to a sediment response in longer period range. The following analysis is then used to target EHVSR to estimate velocity structure model.

The black line in Fig. 3a shows the calculated EHVSR from underground velocity structure model using the diffuse field theory (Kawase et al. 2011). The calculated EHVSR agrees well with the observed EHVSR in gray line. Simulated annealing (SA, Ingber 1989) is applied to search the suitable model. Out of the 200 initial models generated within the search range by

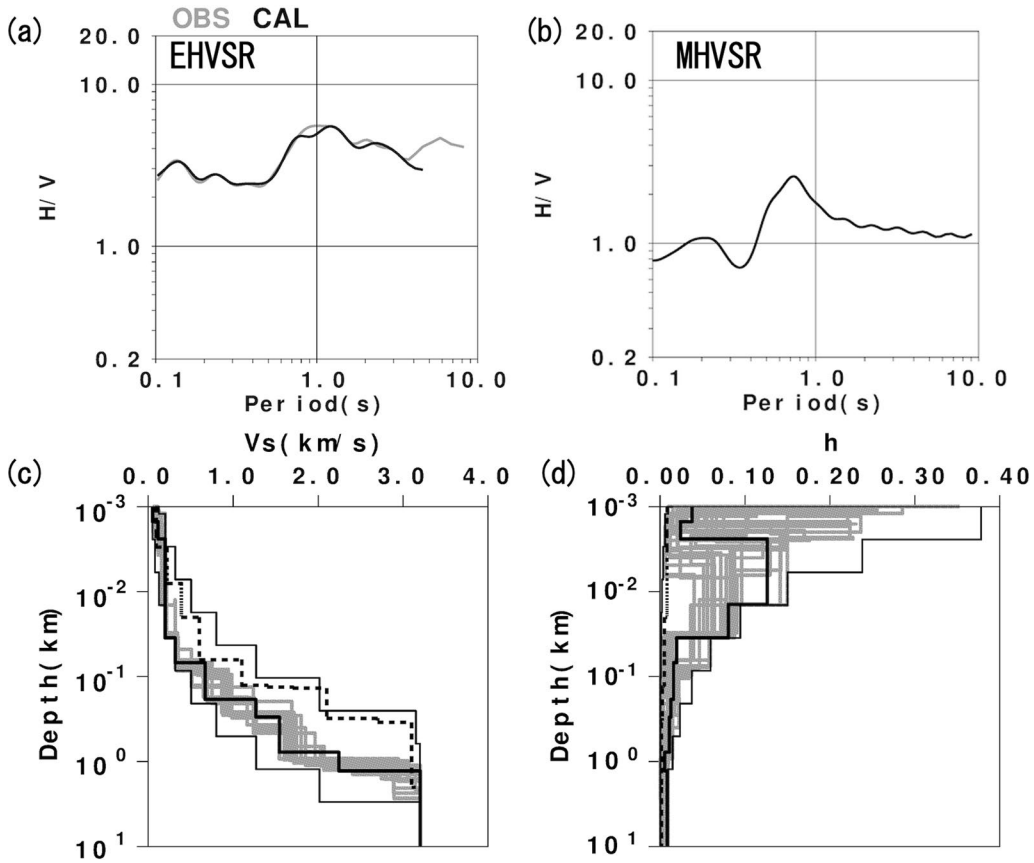

Fig. 3 Observed and calculated *H/V* of earthquake ground motion with estimated underground structures. **a** Observed (gray) and calculated (black) EHVSR at TTR002 site. **b** Observed MHVSR near the TTR002 site. **c** S wave velocity model with the results of 21 cases performed with different initial random numbers (gray lines), the most suitable solution (bold line) from which black line of (**a**) is calculated, and the search range (thin solid lines). Detailed parameters of the most suitable solution are shown in Additional file 1: Table S1. The dashed line indicates J-SHIS model (National Research Institute for Earth Science and Disaster Resilience 2019b) with PS-logging data at TTR002 site. **d** Same as (**c**) but for attenuation model

random numbers, 20 models with small differences from the observation remain. Around the parameters of 20 models, new parameters for next step are randomly generated in the range corresponding to the temperature at respective step. In addition, a hybrid heuristic search is performed by considering the genetic algorithm (GA, Holland 1975) to allow crossing of parameters in each layer. A 200-step SA search is carried out while lowering temperature so that the integrated area of difference between observation and calculation in the spectral figure is minimized. After 21 trials with different initial values of pseudo-random number, the most suitable model is proposed.

Estimated velocity structure

Figure 3c, d show the results of 21 cases that were evaluated with different initial values of pseudo-random number in gray lines. The most suitable solution is shown in bold line, and the search range in thin solid lines. In the analysis, S wave velocity and attenuation h are used as the target physical parameters. Here, attenuation h is used instead of quality factor Q, but there is a relationship of $Q=(2\ h)^{-1}$ between the two parameters. The other parameters, P wave velocity and density, are evaluated from the S wave velocity using empirical formulas. The relation provided by Kitsunezaki et al. (1990) is used to evaluate P wave velocity from S wave velocity, while the relation provided by Gardner et al. (1974) is used to estimate density from P wave velocity. The search range is set as follows. The minimum and maximum S wave velocities are set as 0.005 and 3.2 km/s. The maximum depth is initially given as 3.0 km. The depth and S wave velocity are approximated as a linear function in both logarithms, and the initial model is set by dividing the sediment layer into nine layers equally in logarithmic scale, and minimum and maximum values of the divided portions are included in the searching range. Dashed lines

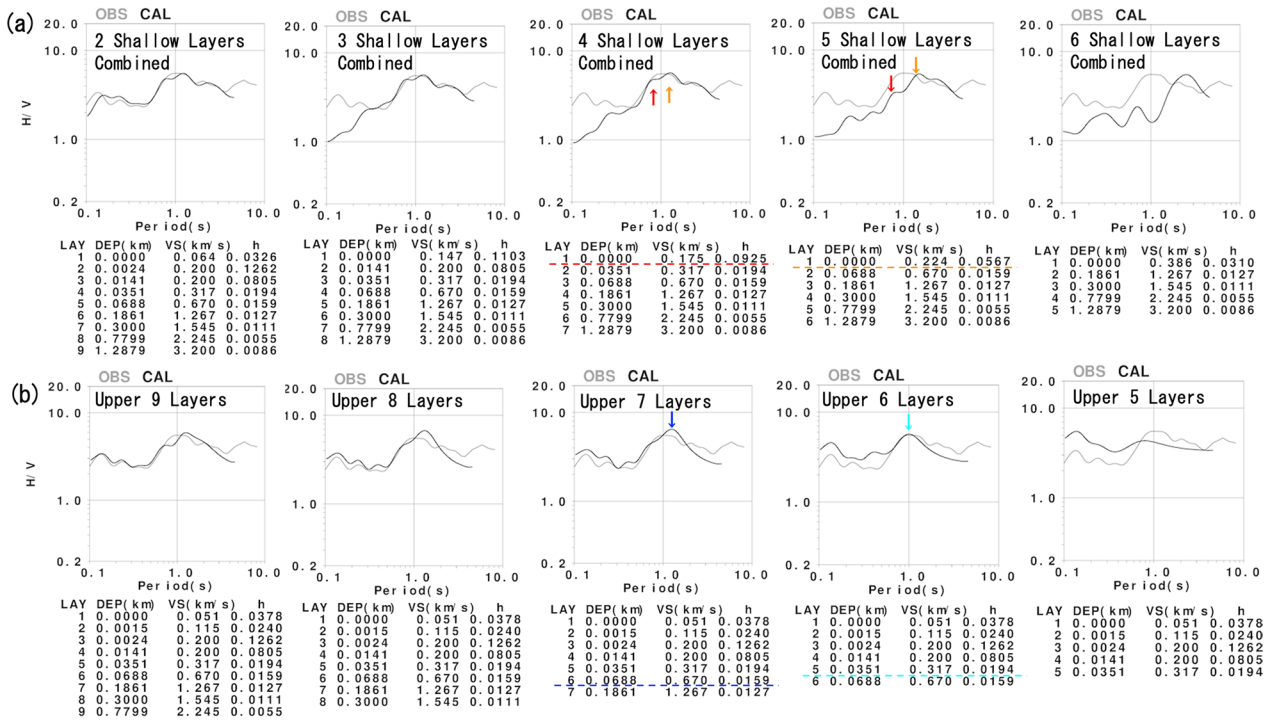

Fig. 4 **a** Calculated EHVSR by combining the surface layers in order from the shallow layer with evaluated average S wave velocity of target layers. Red and orange arrows and dashed lines indicate the characteristic periods and the layer boundaries that compose them. **b** Same as upper row but for removing the deepest layer from the previous model. Blue and sky arrows and dashed lines also indicate the characteristic periods and the layer boundaries that compose them

in Fig. 3c, d show the J-SHIS model (National Research Institute for Earth Science and Disaster Resilience, 2019b) with K-NET PS-logging data at TTR002 which is also included in the search range. However, it is difficult to interpret the observed data with the model because of insufficient survey information in the area.

Figure 3a shows calculated (black) EHVSR from the most suitable solution (Additional file 1: Table S1) with observed (gray) EHVSR. EHVSR around the predominant period of 1 s appears to be composed of two small peaks.

Discussion

The layer boundary corresponding to the predominant period of the observed EHVSR has been studied. First, we started the study by combining shallow layers. Figure 4a shows the results of calculated EHVSR by combining the surface layers in order, beginning from the shallowest layer and obtaining the average S wave velocity of combined layer in the same way as for AVS30 evaluation (Joyner and Fumal 1984). P wave velocity and density of the combined layer are evaluated again from the S wave velocity using empirical formulas, and the attenuation is set by a weighted average according to the layer thickness.

In the left panel of Fig. 4a, the first and second surface layers are combined, "2 Shallow Layers Combined," and it is suggested that the predominance of 0.1–0.2 s is affected by the first layer. Combined from the first layer to the third, "3 Shallow Layers Combined," the predominance of 0.3 s or less disappears. This period range might be affected by the surface layers that are shallower than about 14 m. In "5 Shallow Layers Combined" and "6 Shallow Layers Combined" also, shorter peak of about 0.8 s in the two peaks around 1 s becomes smaller (left down arrow) than that of "4 Shallow Layers Combined" model (left up arrow). This period range might be influenced by shallower sediments having thickness of about 35 m over the engineering bedrock with Vs = 0.317 km/s. It is found that the peak of longer than 1 s still remains in "5 Shallow Layers Combined" case (right down arrow), however, it is slightly extended compared to the case of "4 Shallow Layers Combined". The boundary of top layer having Vs = 0.670 km/s also has effects on the peak around 1 s.

We have also tried to make the base layer shallower by removing the deepest layer of the prior model. The results are shown in Fig. 4b. The "Upper 9 Layers" in left panel is almost the same as the original in Fig. 3a, and may have no effect even if the base layer having

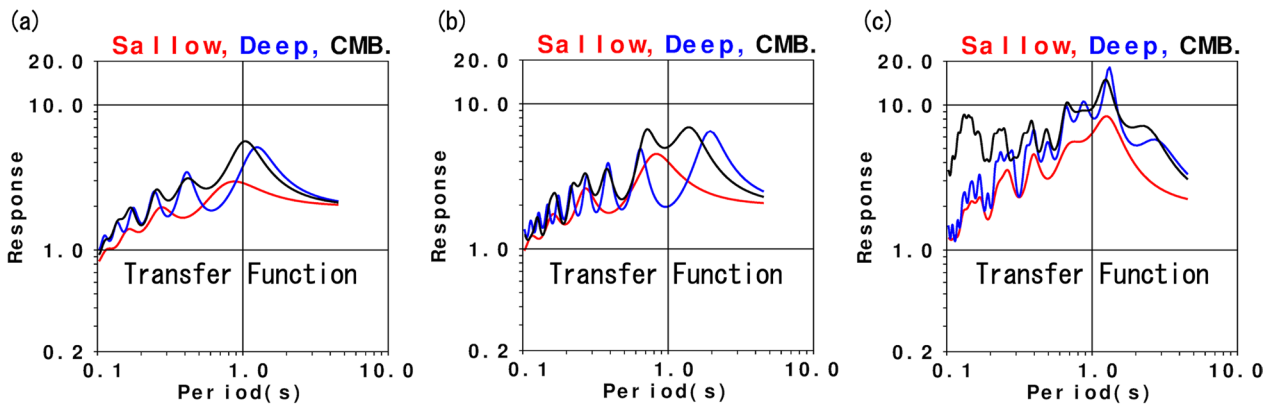

Fig. 5 Calculated site amplifications from simple multi-layer models. **a** Combined model is a 3 layer model from averaged shallow 4 layers in Fig. 4a as the first layer with two deeper layers down to Vs of 0.67 km/s as indicated in Additional file 1: Table S2a, shallow model is composed from the top two layers of the combined model and the two layers of deep model is composed from averaged shallow two layers of the combined model with basement (Additional file 1: Table S2a). **b** Same as the panel (**a**) but combined model is composed by changing the second layer to an averaged layer of deeper two layers of combined model in panel (**a**) and adding next deep layer with Vs of 1.267 km/s as the third layer (Additional file 1: Table S2b). **c** Combined model is total 10 layer model as shown in Fig. 3 and Additional file 1: Table S1, shallow model is a four layer model with a combination of the two combined model in panels (**a**) and (**b**), deep model has two base layers that have Vs of 1.759 km/s as an average of deeper layers and Vs of 3.2 km/s as the seismic bedrock (Additional file 1: Table S2c)

Vs = 3.2 km/s is set to Vs = 2.245 km/s in the target period range. It is shown that the outline of observed EHVSR can be almost expressed until "Upper 7 Layers" model. In the "Upper 6 Layers" model, the peak slightly longer than 1 s becomes unclear, however, the notable peak around 1 s still remains. This peak corresponds to the shorter peak indicated by left arrows in the shallow layers combined model in Fig. 4a. The peak around 1 s might have been generated by the shallower five sedimentary layers, "Upper 6 Layers" model, and is slightly amplified with the addition of 7th layer having Vs = 1.267 km/s, "Upper 7 Layers" model.

Next, site amplifications, transfer functions of SH wave, are calculated from the simplified layered model by combining four shallow layers as shown in Fig. 4a. The black line in Fig. 5a shows the amplifications of a three layered model with Vs of bottom layer being 0.67 km/s as the combined model. The detailed model parameters in Fig. 5 are shown in Additional file 1: Table S2. The red and blue lines indicate the effects of shallower two layers of the combined model and averaged shallow two layers with bottom layer of the combined model respectively. It is shown that both the two boundaries of top layer having Vs = 0.317 km/s and 0.670 km/s compose the peak around 1 s. The result indicates that the two high impedance boundaries with Vs 0.317 km/s and 0.670 km/s compose high amplification around 1 s.

Combined model in Fig. 5b is created by the same way as in Fig. 5a but for changing the second layer to an averaged layer of deeper two layers of combined model in Fig. 5a and adding next deep layer as the third layer (Additional file 1: Table S2a, b). The peak in shallow model is amplified because Vs of bottom layer changes more than the case shown in Fig. 5a. It shows that the effect of shallow soft sediments is important to generate the peak around 1 s. The combined model explains the high amplification around the period of 1 s. However, predominant periods of deep model do not match the peak around 1 s and may create a trough at the period of 1 s in the combined model. The results suggests that the boundary with top Vs = 1.267 km/s contributes only for amplification but not for the peak period.

The combined model in Fig. 5c is the same as the 10 layer model obtained in Fig. 3 and Additional file 1: Table S1, and the model is expected to explain the observed amplification. The shallow model in same panel is composed by the typical four layer model as in the previous analysis in Fig. 5a, b, also in Additional file 1: Table S2a, b. In deep model, the base layer of shallow model is replaced by one averaged sedimentary layer below the 0.1861 km depth of combined model (7–9 layers in Additional file 1: Table S1) with seismic bedrock having Vs = 3.2 km/s. Amplification of deep model almost completely agrees with that of the combined model around 1 s. The shallow model also explains peak period and the shape of amplification around 1 s except for its level.

From the analyses performed above, all the combined models in Fig. 5a, b (Additional file 1: Table S2a, b) and the shallow model in Fig. 5c (Additional file 1: Table S2c) show peak around 1 s, but the simplest

model that has the peak period of interest is the combined model in Fig. 5a with three simple layers. The amplification level agrees with the total 10 layer model after addition of deeper layers below the three layer model.

Thus, in Tottori plain, the effect of shallow soft layers sedimented after the last ice age appears around 1 s, and another peak around this period is generated by the effect of a deeper high contrast boundary. The effects are combined and create larger peak amplification in site response. The deep velocity structure down to the seismic bedrock has effects on the amplification level but does not on the predominant period itself around 1 s. The predominant period is affected by shallower high contrast boundary than the seismic bedrock at TTR002 site. It is considered that such a phenomenon can occur in other small plains along the coast of the Sea of Japan that have similar formation processes.

Conclusion

The underground velocity structure is estimated by applying the diffuse field theory (Kawase et al. 2011) to EHVSR in the Tottori plain, and the layer boundary explaining the predominant period is examined. The conclusions derived from the study are as follows:

1. Stable EHSVR is derived from six records at K-NET TTR002 site, and large peak around 1 s is indicated.
2. Velocity structure under TTR002 site is estimated from EHSVR by employing a hybrid holistic search technique with diffuse field theory (Kawase et al. 2011).
3. The peak around 1 s estimated in the Tottori plain is generated by two different layered boundaries beneath the shallow soft layer with Vs = 0.175 km/s. One is the engineering bedrock with top Vs of 0.317 km/s, and the other is a deeper high contrast boundary with top Vs of 0.67 km/s.
4. The deeper boundaries with top Vs of 1.267 km/s and higher have effects on the amplification level of the peak.

Such a phenomenon may occur in other small plains along the coast of the Sea of Japan, since they have similar formation processes, and the conclusions derived here will be useful in considering future earthquake disaster prevention in them.

Abbreviations

H/V: Horizontal components over vertical component; EHVSR: *H/V* derived from earthquake ground motions; MHVSR: *H/V* derived from microtremor records; K-NET: Kyoshin (strong motion in Japanese)-NETwork maintained by National Research Institute for Earth Science and Disaster Resilience; J-SHIS: Japan Seismic Hazard Information Station; PGA: Peak ground acceleration.

Supplementary Information

The online version contains supplementary material available at https://doi.org/10.1186/s40623-022-01640-3.

Additional file 1: Table S1. Detailed parameters of the most suitable solution in Fig. 3c, d. **Table S2.** Detailed parameters to calculate site amplifications in Fig. 5a–c.

Acknowledgements

The authors appreciate NIED (the National research Institute for Earth science and Disaster Prevention) for providing strong ground motion data at TTR002 and underground structure model. The authors also appreciate accurate and fruitful comments by the guest editor and the two reviewers, and English language review by Enago (www.enago.jp).

Author contributions

TK made analysis of strong ground motion records and TN conducted microtremor observations and integrated the results. After discussion among authors, TK drafted the manuscript. All authors read and approved the final manuscript.

Funding

This study was partially supported by Ministry of Education, Culture, Sports, Science and Technology (MEXT) of Japan, under its The Second Earthquake and Volcano Hazards Observation and Research Program (Earthquake and Volcano Hazard Reduction Research).

Availability of data and materials

Strong motion data at K-NET TTR002 are available from National Research Institute for Earth Science and Disaster Resilience (NIED) at http://www.kyoshin.bosai.go.jp (last accessed September 2021). Microtremor observation data conducted around TTR002 site are available on contacting the authors.

Declarations

Ethics approval and consent to participate

Not applicable.

Consent for publication

Not applicable.

Competing interests

The authors declare that they have no competing interests.

Received: 30 September 2021 Accepted: 3 May 2022
Published online: 23 May 2022

References

Bonilla LF, Liu P-C, Nielsen S (2006) 1D and 2D linear and nonlinear site response in the Grenoble area, Third International Symposium on the Effects of Surface Geology on Seismic Motion, Paper Number: 082/S02

Furumura T, Kennett BLN, Koketsu K (2003) Visualization of 3D wave propagation from 2000 Tottori-ken Seibu, Japan, earthquake: observation and numerical simulation. Bull Seism Soc Am 93(2):870–881

Gardner GHF, Gardner LW, Gregory AR (1974) Formation velocity and density—the diafnostic basics for stratigraphic traps. Geophysics 39(6):759–918

Holland JH (1975) Adaptation in natural and artificial systems. The University of Michigan Press, Ann Arbor

Idriss IM (1991) Earthquake ground motions at soft soil sites, International conference on recent advances in geotechnical earthquake engineering and soil dynamics 3

Ingber L (1989) Very fast simulated annealing. Math Comput Modeling 12:967–973
Joyner W, Fumal T (1984) Use of measured shear-wave velocity for predicting geologic site effects on strong ground motion, Proc. 8th World Conf. on Earthq. Eng. 777–783
Kagawa T, Zhao B, Miyakoshi K, Irikura K (2004) Modeling of 3D basin structures for seismic wave simulations based on available information on the target area: case study of the Osaka basin, Japan. Bull Seism Soc Am 94(4):1353–1368
Kanno T, Miura K (2006) Earthquake response characteristics of small sedimentary basin, Proc. 12th Japan Earthq. Eng. Symp. 306–309
Kawase H, Sánchez-Sesma FJ, Matsushima S (2011) The optimal use of horizontal-to-vertical spectral ratios of earthquake motions for velocity inversions based on diffuse-field theory for plane waves. Bull Seism Soc Am 101(5):2001–2014
Kitsunezaki C, Goto N, Kobayashi Y, Ikawa T, Horike M, Saito T, Kuroda T, Yamane K, Okuzumi K (1990) Estimation of P- and S- wave velocities in deep soil deposits for evaluating ground vibrations in earthquake". J Nat Disaster Sci 9(3):1–17 (**in Japanese with English abstract**)
Konno K, Ohmachi T (1995) A smoothing function suitable for estimation of amplification factor of the surface ground from microtremor and its application. J Japan Soc Civ Eng 524(I–33):247–259 (**in Japanese with English abstract**)
National Research Institute for Earth Science and Disaster Resilience (2019a) NIED K-NET KiK-Net. Nat Res Inst Earth Sci Disaster Resilience. https://doi.org/10.17598/NIED.0004
National Research Institute for Earth Science and Disaster Resilience (2019b) J-SHIS shallow and deep layers combined model (SDLCM). Nat Res Inst Earth Sci Disaster Resilience. https://doi.org/10.17598/NIED.0012
Tsai VC, Bowden DC, Kanamori H (2017) Explaining extreme ground motion in Osaka basin during the 2011 Tohoku earthquake. Geophys Res Lett 44(14):7239–7244
Uetake T, Kudo K (2005) Assessment of site effects on seismic motion in Ashigara valley, Japan. Bull Seism Soc Am 95(6):2297–2317
Yamanaka H, Yamada N (2006) Modeling 3D S-wave velocity structure of Kanto basin for estimation of earthquake ground motion. BUTSURI-TANSA 59(6):549–560 (**in Japanese with English abstract**)
Yoshimoto K, Takemura S (2014) A study on the predominant period of long-period ground motions in the Kanto basin. Earth Planets Space 66:100. https://doi.org/10.1186/1880-5981-66-100

Publisher's Note